Non-invasive characterization of particle morphology of calcareous sands from São Tomé & Príncipe

Ryan Beemer[1], *Joana* Fonseca[2], and *Jeremy* Shaw[3]

[1]*University of Massachusetts Dartmouth, Department of Civil and Environmental Engineering, Dartmouth, MA 02747, USA*
[2]*City, University of London, Department of Civil Engineering, London EC1V 0HB, UK*
[3]*Centre for Microscopy, Characterisation & Analysis, University of Western Australia, Crawley 6009*
[#]*Corresponding author:* joana.fonseca.1@city.ac.uk

ABSTRACT

Calcareous sands of biogenic origin are widely spread throughout the world's seabed. They are the foundation soils for many offshore geotechnical structures, and, in addition, onshore uses of this material are becoming more significant with the growing demand of backfill material for transport infrastructure. These sands comprise the remains of marine organisms such as shells and tests, and the grains can vary from platy to hollow thin-walled forms with highly angular features. Geotechnical design on calcareous sands is challenging owing to the many uncertainties related to their micro-scale properties. This study uses non-invasive X-ray micro-computed tomography (µCT) and advanced three-dimensional (3D) image analysis techniques to quantify the morphology of bioclastic calcareous sands from São Tomé & Príncipe. The statistics of particle shape parameters of the São Tomé sand are compared to that of the previously studied Ledge Point sand. In spite of an order of magnitude difference in particle size, São Tomé and Ledge Point sands are markedly similar and, as seen in other calcareous sand, São Tomé shows a strong correlation in 3D sphericity and convexity. The results presented here help to better understand the mechanisms of grain interlocking, and the role of intra-granular void ratio on the mechanical behaviour of calcareous sands from different parts of the world.

Keywords: Calcareous sand; Particle shape; Micro-scale; X-ray tomography

1. Introduction

Calcareous sands of biogenic origin comprise for the most part shells and skeletons of small organisms (e.g. Semple 1988; Coop 1990; Kong and Fonseca 2019). Owing to the interlocking of the angular grains and the high intra-granular voids, these sands tend to form a very loose fabric. The complex microstructure of these soils and the associated challenges in extracting meaningful measurements at the particle-scale may explain why their mechanical response is still poorly understood.

Advanced imaging techniques, such as X-ray microtomography offer a powerful tool to access the internal microstructure of these sands in a non-invasive way and quantify the morphology of the particles in terms of size and shape.

The distribution of particle sizes and the grain shapes are fundamental characteristics of a soil. The particle size distribution (PSD) influences the range of attainable void ratios (e.g. Miura et al. 1997) and is a key aspect affecting the soil response, for example at the same relative density a better graded soil may have a larger angle of internal friction (e.g. Holtz and Kovacs 1981). The influence of particle shape on the macro mechanical response of sand derives from the inter-granular stress transmission mechanisms (Zuriguel et al., 2007; Fonseca et al. 2016; Kong and Fonseca 2018). The non-convexities and angularities of shells tend to promote 'interlocking', which reduces the degrees of freedom at the contacts (Frossard 1979) and prevents the grains from slippage (Santamarina and Cho 2004).

In this paper, calcareous sands from two regions of the world, Australia and São Tomé & Príncipe are imaged using 3D x-ray microtomography and the size and shape of the particles quantified. The correlations between the various shape parameters, such as, aspect ratio, convexity, and sphericity are investigated and put forward as important properties that can inform their macro-scale behaviour.

2. 3D X-ray microtomography and analysis

2.1 Sands in the study

The primary focus of this study is the calcareous sand from São Tomé & Príncipe, Fig. 1. This sand was collected as part of the preparatory work for expansion of the international airport located in the northeast coast of São Tomé island. The sand consists, for the most part, of shell fragments, sponge spicules, coral, gastropods and foraminifers (DGRNE 2022). Only a very low percentage, less than 4% is of detritic nature. The carbonate content of the sand varies between 85 to 100%.

The coastal bioclastic sand from Ledge Point, Western Australia, Australia, Fig. 2 is used here for comparison purposes. This sand has been investigated previously (Beemer et al. 2018; Li et al. 2021; Sharma and Ismail 2006) including an X-ray micro-computed tomography (µCT) study (Beemer et al. 2022). The sand

has a carbonate content of 91% and consists largely of plate grains, some hollow foraminifera tests, mollusk shells and bryozoans.
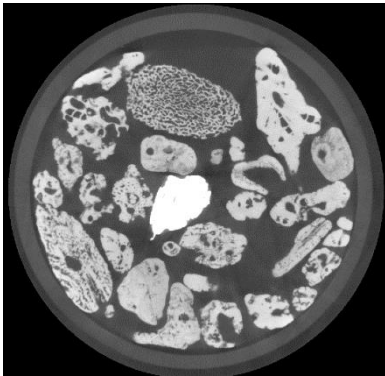

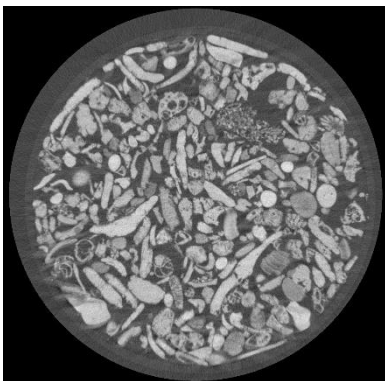**Figure 1.** X-ray microtomography scan of São Tomé sand in a 30 mm diameter tube.

Figure 2. X-ray microtomography scan of Ledge Point sand in a 5 mm diameter tube.

2.2 Image acquisition

São Tomé & Príncipe sediment was poured into a 30mm diameter plastic tube and placed onto the stage of the μCT scanner (Versa 520 XRM, Zeiss). The sample was scanned at 140kV, 10W (71.5 μA) using an HE2 beam filter. Source and detector positions were set to -59 and 75 mm, respectively, and the 0.4X macro objective with 2x camera binning yielded a final pixel resolution of 30.39 μm. An exposure of 3s was used for each of the 2400 projection images through 360º of rotation. Automatic reconstruction was used with Scout and Scan Reconstructor (v15.0.17350.39816).

2.3 Image processing

The initial μCT images, Fig. 3, were pre-processed to improve image contrast. The MATLAB® ver. R2021b function `imsharpen` with a radius of thirty pixels and the function `imerode` with a size of one pixel were applied to each grayscale slice. Each image was then binarized using Otsu's method (Otsu 1979), Fig. 4. The function `imfill` was applied along each of the three dimensions to fill enclosed voids. Finally, `imopen` with a two-pixel sphere mask was used to remove small artefacts.

A watershed segmentation algorithm was used to separate the individual grains in 3D. The watershed algorithm was developed by Kong and Fonseca (2018) and improved for computational speed with branch recursive processing by Leonti et al. (2020). The volume was split into four sections along its y-axis and processed in quarters to optimize memory usage. Each section overlapped its neighbour by 1/6th its length to ensure continuity. After segmentation the pixels added during infilling were removed to create the final segmented volume, Fig. 5.
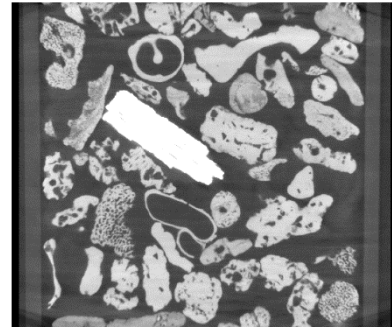

Figure 3. X-ray microtomography scan of São Tomé sand in a 30 mm diameter tube, prior to binarization.

Figure 4. Sharpened and threshold, using Otsu method, image of the São Tomé sand in a 30 mm diameter tube.

Figure 5. Segmented São Tomé sand. A slight over segmentation can be seen in a 30 mm diameter tube.

2.4 3D particle shape parameters

The 3D shape parameters used to analyze the particles from the segmented μCT images are summarized below. ESD diameter (d_{ESD}) is the parameter representing the diameter of a sphere having an equivalent volume to the particle under consideration:

$$d_{ESD} = \sqrt[3]{\frac{6V}{\pi}}$$

Feret-length, Feret-width, and Feret-thickness ($d_{Flength}$, d_{Fwidth}, $d_{Fthickness}$) describe the longest, intermediate, and shortest dimensions of a soil particle (D18 Committee 2016; Krumbein 1941). The ferret dimensions were obtained with a principal coordinate analysis (PCA) through the `regionprop3` and `pcacov` functions in the same software.

In 3D, there are three different aspect ratio parameters that are typically calculated, including thickness-to-length ratio, elongation index, and flatness index (Zingg 1935). In this study only, the thickness-to-length ratio (AR_{3D}) parameter is investigated:

$$AR_3 = \frac{d_{Fthickness}}{d_{Flength}}$$

Sphericity (S_{3D}) is defined from (Wadell 1935) as the ratio of the surface area of a volume equivalent sphere to a surface area of a real particle (A_s):

$$S_{3D} = \frac{\pi d_{ESD}^2}{A_s}$$

Convexity (C_{x3D}) in 3D is defined as the volume of the solid shell (V) divide by the volume of the convex hull (V_c) (ISO 2008):

$$C_{x3D} = \frac{V}{Vc}$$

3. Results

3.1. Particle size distribution (PSD)

The particle size distribution from the 3D μCT is provided in Fig. 6. It includes the d_{ESD} and the Feret range ($d_{F\text{-}length} - d_{F\text{-}thickness}$). The digital PSD were constructed with bin edges set to values typical of mechanical sieve sizes: 0.15, 0.18, 0.425, 0.60, 1.18 2.36, 4.75, 12.5, 25, 75, and 100 mm.

The equivalent spherical diameter falls in the middle of the Feret range. The Feret range is relatively large indicating a significant difference between the length and thickness of the particles. The São Tomé sand was considerably coarser than the Ledge Point sand with a D_{50} (median grain size) of 3.8 mm versus 0.38 mm. This difference is evident when comparing the μCT scans in Figs. 1 and 2, respectively.
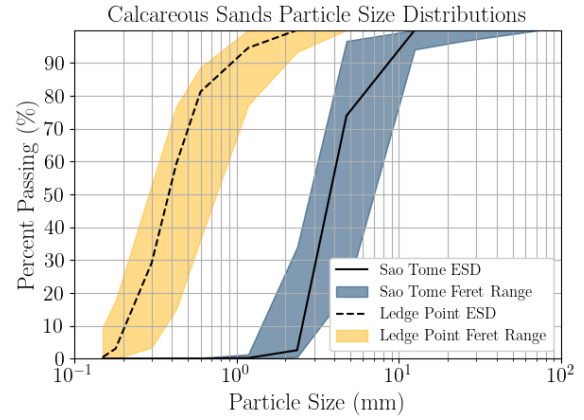

Figure 6. Particle size distribution of the São Tomé and Ledge Point sands, equivalent spherical diameter (ESD) and Feret range.

3.2. Statistics of particle shape

Probability density plots of the shape parameters AR_{3D}, S_{3D}, and Cx_{3D} of São Tomé sand are provided in Figs. 7-9. All three histograms appear non-normal and exhibit significant skew. The medians of aspect ratio, sphericity, and convexity of the São Tomé sand are 0.43, 0.42, and 0.64 respectively. In comparison, the Ledge Point sand medians are 0.43, 0.62, and 0.64, respectively. The distributions of aspect ratio and convexity are similar to those of the Ledge Point sand, but Ledge Point has a significantly higher sphericity and is less skewed.
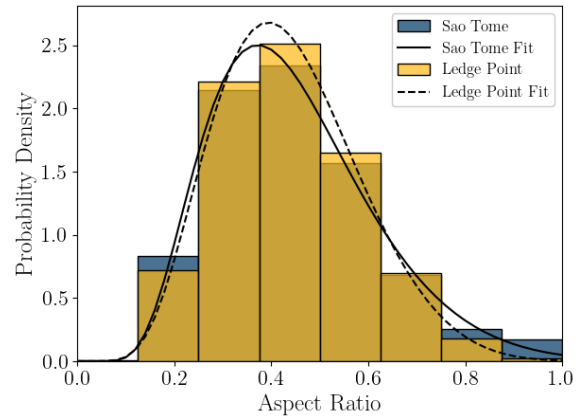

Figure 7. Distribution of 3D Aspect Ratio of São Tomé and Ledge Point sands.
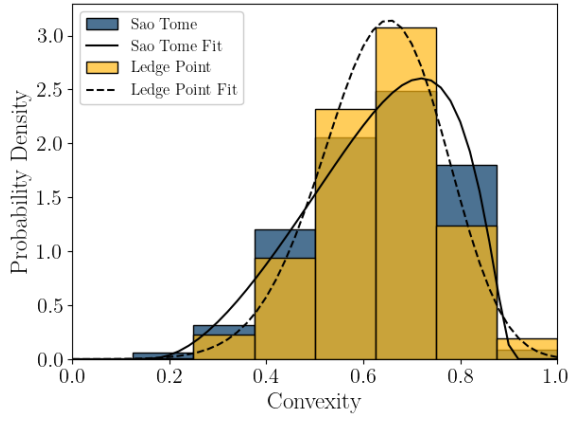
Figure 8. Distribution of 3D Convexity of São Tomé and Ledge Point sands.
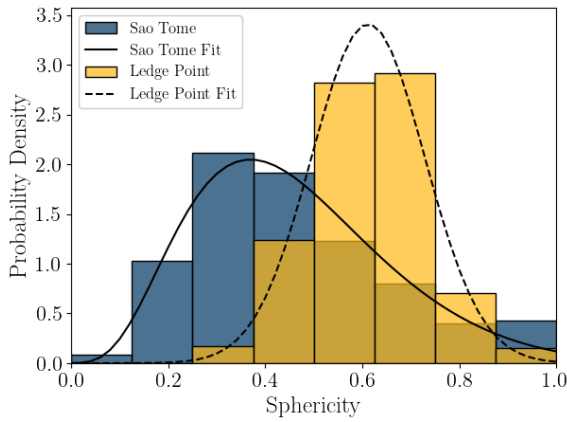

Figure 9. Particle size distribution of the São Tomé and Ledge Point sands, equivalent spherical diameter (ESD) and Feret range.

Given the skewed nature of the histograms they were fitted with (Johnson, 1949) fit line in Figs. 7-9. The Johnson Distributions are used for fitting non-normal geotechnical parameters (Ching and Phoon 2015). The Bounded Johnson's Distribution limits the range of the random variable to $0 \leq x \leq 1$ which matches the normalized definitions of the particle shape parameters. Its probability density function can be defined by:

$$f(x) = \frac{\delta}{(x-\xi)\left(1-\frac{x-\xi}{\gamma}\right)} \Phi\left(\gamma + \delta \cdot ln\left(\frac{x-\xi}{\lambda+\xi-x}\right)\right)$$

where: Φ is the normal distribution probability density function, x is an independent random variable, δ and γ are fitting parameters, ξ is the location variable, and λ is the scaling variable.

The SciPy distribution fitting function (Virtanen et al. 2020) was used to obtain the four Johnson fitting parameters for the shape parameters AR_{3D}, Cx_{3D}, and S_{3D} for the Ledge Point bioclastic calcareous sand in Table 1.

Table 1. Johnson's Distribution fitting variables to 3D shape parameters

	Aspect Ratio (AR_{3D})	Convexity (Cx_{3D})	Sphericity (S_{3D})
	3D Johnson Bounded Distribution		
γ:	1.9481	-0.7179	2.3239
δ:	1.7465	1.0854	1.8764
ξ:	-0.0406	0.1283	0.0190
λ:	1.9200	0.7929	1.8009

3.3. Correlation of particle shape

A correlation coefficient analysis was conducted on both the shape parameters and the equivalent spherical diameter, Table 2. These results are also presented graphically as correlation plots, Figs. 10-12. The strongest correlations of shape parameters are of S_{3D} with d_{ESD}, -0.70 and S_{3D} with Cx_{3D}, 0.71. These are associated with the tightest grouping of points in Fig. 12. Ledge Point sand also has a strong correlation of S_{3D} with Cx_{3D}, 0.72, but S_{3D} with d_{ESD} are not strongly correlated, -0.48.

Table 2. Correlation coefficient for 3D shape parameter of São Tomé sand

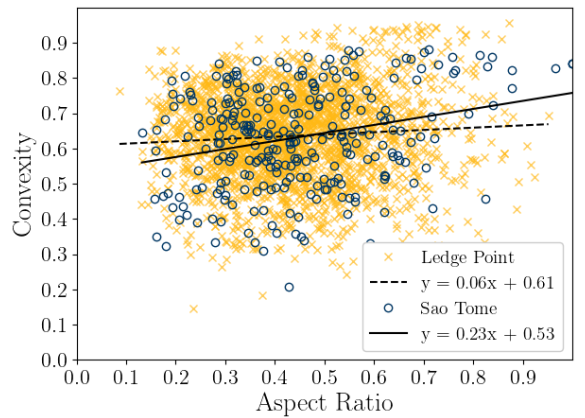|	d_{ESD}	AR_{3D}	C_{x3D}	S_{3D}
d_{ESD}	1	—	—	—
AR_{3D}	-0.28	1	—	—
C_{x3D}	-0.41	0.27	1	—
S_{3D}	-0.70	0.27	0.71	1

Figure 10. Correlation of convexity versus aspect ratio for São Tomé and Ledge Point sands.
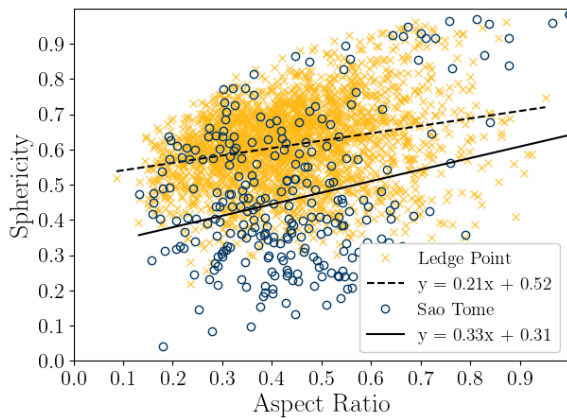
Figure 11. Correlation of Sphericity versus Aspect Ratio for São Tomé and Ledge Point sands.
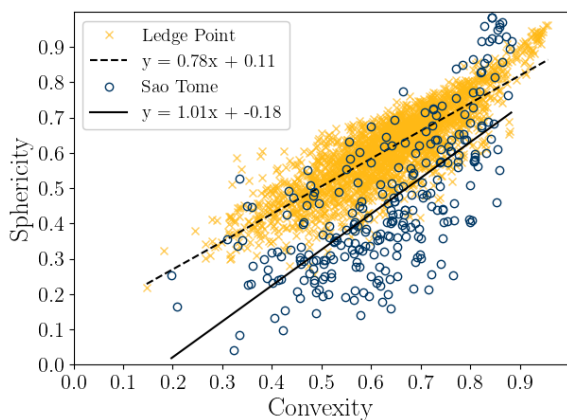

Figure 12. Correlation of sphericity versus convexity for São Tomé and Ledge Point sands.

4. Discussion

In spite of there being an order of magnitude difference in the D_{50} and from being on the other side of the Earth from each other the São Tomé and Ledge Point sands they have very similar statistics of particle shape parameters. This is likely due to their similar biological origin and environment in which they were from. The only significant difference being that the São Tomé is less spherical. This could be a function of the particle size. Since both sands are of similar, but not exact, biological origin size of the sand grains would be a function of physical weathering. As large platy and angular particles, e.g. shells, undergo fracture their sphericity will increase. The particle size and sphericity are strongly correlated in the São Tomé, Table 2, but not in Ledge Point. This seems reasonable if calcareous particles are self-similar when fractured.

As seen in other calcareous sands (Beemer et al. 2022; Li et al. 2021; Rorato et al. 2019), three-dimensional sphericity is strongly correlated to convexity. Beemer et al. (2022) argued this was due to the biomorphology of the sand grains. Intact shells, tests, or coral will have low sphericity and convexity. As they undergo physical weathering from wind and waves their Feret dimensions should tend towards unity since any

applied moment would be largest across the longest particle dimension. Therefore, bioclastic sands would have large young particles with low sphericity and small older ones with high sphericity. The strong correlation of sphericity and size in the São Tomé sand, Table 2, seems to support this hypothesis.

5. Conclusions

The following conclusions can be drawn from this μCT study on the São Tomé bioclastic calcareous sand and comparison to Ledge Point coastal bioclastic calcareous sand.

1. Bounded Johnson distributions of aspect ratio, sphericity, and aspect ratio for the São Tomé sand have been provided. These may be useful for future modelling of these calcareous sands.
2. The D_{50} of the São Tomé is an order of magnitude larger than the Ledge Point calcareous sand from Western Australia, but have similar statistical distributions of convexity and aspect ratio, Figs.7-8. The São Tomé sand was less spherical than the Ledge Point sand, median of 0.42 vs 0.62 respectively. This could be a factor of the grain size.
3. Sphericity and convexity appear to be strongly correlated, 0.70, in the São Tomé calcareous sand, Table 2. This is similar to other calcareous sands reported in the literature.

References

Beemer, R. D., Bandini-Maeder, A. N. Shaw, J. Lebrec, U., Cassidy, M. J., 2018. "The granular structure of two marine carbonate sediments." *Proc OMAE2018*. Madrid: ASME.

Beemer, R. D., Li, L., Leonti, A., Shaw, J., Fonseca, J., Valova, I., Iskander, M., Pilskaln, C. H., 2022. "Comparison of 2D Optical Imaging and 3D Microtomography Shape Measurements of a Coastal Bioclastic Calcareous Sand." *J. Imaging*, 8 (3): 20.

Ching, J., Phoon. K.-K., 2015. "Constructing multivariate distributions for soil parameters." *Risk Reliab. Geotech. Eng.*, 3–76. Taylor & Francis Boca Raton, FL.

Coop, M. R., 1990. The mechanics of uncemented carbonate sands. *Géotechnique* 40, No. 4, 607–626, http://dx.doi.org/10.1680/geot.1990.40.4.607.

D18 Committee. 2016. *Standard Practice for Characterization of Particles;* Standard. West Conshohocken, PA, USA,: ASTM.

DGRNE - Direcção Geral dos Recursos Naturais e Energia São Tomé & Príncipe - technical report, "Tipos de solos e suas classificações" https://dgrne.org/directorate/directorate-geology, accessed August 2022

Fonseca, J., Nadimi, S., Reyes-Aldasoro, C. C., O'Sullivan, C., Coop, M. R., 2016. Image-based investigation into the

primary fabric of stress transmitting particles in sand. *Soils Found.* 56, No. 5, 818–834.

Frossard, E.,1979. Effect of sand grain shape on interparticle friction; indirect measurements by Rowe's stress dilatancy theory. *Géotechnique* 29, No. 3, 341–350, http://dx.doi.org/10.1680/geot.1979.29.3.341.

Holtz, R., Kovacs, W., 1981. An Introduction to Geotechnical Engineering. Prentice-Hall, Inc., Englewood Cliffs.

ISO. 2008. *ISO 9276–6 Representation of Results of Particle Size Analysis—Part 6: Descriptive and Quantitative Representation of Particle Shape and Morphology*.

Johnson, N. L. 1949. "Systems of Frequency Curves Generated by Methods of Translation." *Biometrika*, 36 (1/2): 29. https://doi.org/10.2307/2332539.

Kong, D., Fonseca, J. Quantification of the morphology of shelly carbonate sands using 3D images. *Géotechnique* 2018, 68, 249–261. doi:10.1680/jgeot.16.p.278.

Kong, D., Fonseca, J., 2019. On the kinematics of shelly carbonate sand using X-ray micro tomography. Engineering Geology, 261, pp. 105268–105268. doi:10.1016/j.enggeo.2019.105268

Krumbein, W. C., 1941. "Measurement and geological significance of shape and roundness of sedimentary particles." *J. Sediment. Res.*, 11 (2): 64–72. SEPM Society for Sedimentary Geology.

Li, L., R. D. Beemer, and M. Iskander. 2021. "Granulometry of Two Marine Calcareous Sands." *J. Geotech. Geoenvironmental Eng.*, 147 (3): 04020171. https://doi.org/10.1061/(ASCE)GT.1943-5606.0002431.

Miura, K., Maeda, K., Furukawa, M., Toki, S., 1997. Physical characteristics of sand with different primary properties. *Soils and Foundations* 37 (3), 53–64

Otsu, N. 1979. "A threshold selection method from gray-level histograms." *IEEE Trans. Syst. Man Cybern.*, 9 (1): 62–66. IEEE.

Rorato, R., Arroyo, M., Andò, E., Gens. A., 2019. "Sphericity measures of sand grains." *Eng. Geol.*, 254: 43–53. https://doi.org/10.1016/j.enggeo.2019.04.006.

Semple, R.M.,1988. The mechanical properties of carbonate soils. In Engineering for calcareous sediments (eds R. J. Jewell and D. C. Andrews), pp. 807–836. Rotterdam, the Netherlands: Balkema.

Santamarina, J. C., Cho, G. C., 2004. Soil behaviour: the role of particle shape. In Advances in geotechnical engineering: the Skempton conference (eds R. J. Jardine, D. M. Potts and K. G. Higgins), pp. 604–617. London, UK: ICE Publishing.

Sharma, S. S., Ismail, M. A., 2006. "Monotonic and cyclic behavior of two calcareous soils of different origins." *J Geotech Geoenviron Eng Geotech Geoenviron Eng*, 132 (12): 1581–1591. ASCE. https://doi.org/10.1061/(ASCE)1090-0241(2006)132:12(1581).

Virtanen, P., R. Gommers, T. E. Oliphant, M. Haberland, T. Reddy, D. Cournapeau, E. Burovski, P. Peterson, W. Weckesser, J. Bright, S. J. van der Walt, M. Brett, J. Wilson, K. J. Millman, N. Mayorov, A. R. J. Nelson, E. Jones, R. Kern, E. Larson, C. J. Carey, İ. Polat, Y. Feng, E. W. Moore, J. VanderPlas, D. Laxalde, J. Perktold, R. Cimrman, I. Henriksen, E. A. Quintero, C. R. Harris, A. M. Archibald, A. H. Ribeiro, F. Pedregosa, P. van Mulbregt, and SciPy 1.0 Contributors. 2020. "SciPy 1.0: Fundamental Algorithms for Scientific Computing in Python." *Nat. Methods*, 17: 261–272. https://doi.org/10.1038/s41592-019-0686-2.

Wadell, H., 1935. "Volume, shape, and roundness of quartz particles." *J. Geol.*, 43 (3): 250–280. University of Chicago Press. https://doi.org/10.1086/624298.

Zingg, T., 1935. "Beitrag zur Schotteranalyse." PhD Thesis. ETH Zurich (in German).

Zuriguel, I., Mullin, T., Rotter, J. M., 2007. Effect of particle shape on the stress dip under a sandpile. *Phys. Rev. Lett.* 98, No. 2, 028001.